

## Investigating the optical and electrical characteristics of $\text{As}_{60}\text{Cu}_{40-x}\text{Se}_x$ thin films prepared using pulsed laser deposition method

J. S. Mohammed<sup>a\*</sup>, F. K. Nsaif<sup>b</sup>, Y. M. Jawad<sup>a</sup>, K. A. Jasim<sup>b</sup>, A. H. Al Dulaimi<sup>a</sup>

<sup>a</sup>*Department of Physics, College of Science, University of Diyala, Diyala, Iraq.*

<sup>b</sup>*Department of physics, College of Education for pure sciences Ibn Al-Haitham, University of Baghdad, Baghdad, Iraq*

In this work,  $\text{As}_{60}\text{Cu}_{40-x}\text{Se}_x$  thin films were synthesized, and the pulsed laser deposition method was used to study the effected partial replacement of copper with selenium. The electrical characteristics and optical characteristics, as indicated by the absorbance and transmittance as a function of wavelength were calculated. Additionally, the energy gap was computed. The electrical conductivity of the DC in the various conduction zones was calculated by measuring the current and voltage as a function of temperature. Additionally, the mathematical equations are used to compute the energy constants, electron hopping distance, tail width, pre-exponential factor, and density of the energy states in variation zones (densities of the energetic extended states  $N_{(\text{Eext})}$ , localize  $N_{(\text{Eloc})}$  and at the Fermi states  $N_{(\text{EF})}$ ). The acquired data also demonstrated that the selenium concentration obviously had an impact on the electrical conduction mechanics, energy states, and the level of randomization.

(Received March 15, 2023; Accepted July 4, 2023)

*Keywords:* Pulsed laser deposition, Thin film, partial replacement, Optical and electrical properties

### 1. Introduction

In several technological contexts, the pulse laser deposition method is one of the most effective and affordable methods for semiconductor, mineral, and oxide deposits. Despite the fact that the first thin film production using pulse laser technology began in 1960 [1]. The optical features of amorphous semiconductors include unique infrared transmittance ranges and an elevated refractive index (2-4). This is the optical band gap: appropriate for modified devices and applications. In photovoltaic coating, the thin films of chalcogenides were produced. Thin film photovoltaic coatings for chalcogenides have been developed recently for use in photo thermal equipment, solar radiation absorption, sensing, visualization, verification, and display [2]. The use of optoelectronic devices depends heavily on their optical properties. The separation in energy between bar of the valence and bar of the conduction is generally small in semiconductor materials and is close to the thermal energy (KT). If the material is of the negative type (n-type), the concentration of electrons in the conduction band will grow as the semiconductor's temperature rises, or it may increase the concentration of holes in the valence band if the material is of the other positive type (p-type). The atoms of the impurities are ionized in accordance with the kind of impurity by raising the temperature to ambient temperature (energy of the impurities). The process of producing more electrons and holes as a result of excited electrons moving from bar of the valence to bar of the conduction, known as electron-hole generation, occurs if the temperature is raised above that.

The link between electrical conductivity and semiconductor temperature is displayed in the equation.

$$\sigma = \sigma_0 e^{\left(-\frac{\Delta E}{KT}\right)} \quad (1)$$

---

\* Corresponding author: [jafer.mm1967@uodiyala.edu.iq](mailto:jafer.mm1967@uodiyala.edu.iq)  
<https://doi.org/10.15251/CL.2023.207.449>

Transporter are enthusiastic about prolonged states to display activation Energy  $\Delta E$  ( $E_C - E_F$ ) or ( $E_F - E_V$ ), Temperature is T (k), The Boltzmann constant is k .

Electrical conductivity's contribution is mostly influenced by the various temperature ranges to which the semiconductors are subjected , particularly in the case of the semiconductor chalcogenide glass .

At lower temperatures , conductivity may result from electron or hole hopping between near by Fermi level-like local energy states . However , at moderate temperatures, electrical conductivity is determined by the levels of the energy states at the local level band's tails , where the electronic charges are moved by hopping between the local levels in this area . Regarding increased electrical conductivity at high temperatures is situated between the extended energy levels of the conduction and valence beams . As a result , equation 1 often consists of three terms , each of which denotes a conduction mechanism for one of the aforementioned locations . Equation 1 then has the form [3]

$$\sigma = \sigma_{01}e^{(-\frac{E_1}{kT})} + \sigma_{02}e^{(-\frac{E_2}{kT})} + \sigma_{03}e^{(-\frac{E_3}{kT})} \quad (2)$$

It can be used to establish *understanding the connections between temperature range and electrical conductivity* that a semiconductor is exposed to regarding the first term , which stands for the electrical conductivity at high temperatures , the following equation can be used to determine the *density between the two bundles of conduction and valence of the extended energy levels* [4]

$$\sigma_{0ext.} = (\frac{1}{6})e^2a^2V_eN(E_C) \quad (3)$$

Where electron frequency  $V_e = \frac{\hbar}{a^2M}$  and Interatomic space  $a = 0.026 \frac{e^2}{\hbar\sigma_0}$  therefor  $N(E_{ext})$  [5,6]

$$N(E_{ext}) = [\frac{6m}{e^2\hbar}] \sigma_{0ext} \quad (4)$$

The element that originates from the activation energy before the exponent  $\sigma_{02}$  are computed from equation 2 second term , which stands for conductivity at medium temperatures , before computing the density states of local energy in the vicinity of the energy bands' tails . The following equation states

$$N(E_{loc}) = [\frac{6}{e^2V_{ph}R^2}] \sigma_{02} \quad (5)$$

When  $V_{ph}$  indicates the frequency of a phonons , distance R hops between two localized states

when temperatures are lower , it's feasible to compute the density of local energy levels close to the Fermi level by first extracting the activation energy  $E_3$  as well as the pre-exponential component  $\sigma_{03}$  from the third part of equation 2 . The following equation states that

$$\sigma_{03} = (\frac{1}{6})e^2V_{ph}R^2N(E_F) \quad (6)$$

where e is the electron charge , N ( $E_F$ ) represents the state density close to the Fermi level.

$$\text{So, } R = 0.7736 \left[ \frac{\Delta E \alpha^{-1}}{N(E_C)(kT)^2} \right]^{0.25}$$

Where  $\Delta E = E_1 - E_2$ ,  $\alpha^{-1} = 10^{-7} \text{cm}$  (coefficient of optical absorption) while N ( $E_c$ ) indicate the extended state's density .

## 2. Modeling and working methods

In this paper, The preparation of thin films of  $As_{60}Cu_{40-x}Se_x$  involved weighing and transferring suitable amounts of beginning components, including arsenic, copper, and selenium, into quartz ampoules. The beginning components were then combined thoroughly in the ampoules before being squeezed into a single mass and employing pulsed laser deposition technology to deposit it on glass substrates. It does this by guiding pulses from a pulsed Nd:YAG laser counts of 200, 6 Hz repetition rate and an energy of 400 mJ in vacuum of  $2.5 \times 10^{-2}$  mbar. The figure depicts the device's experimental configuration (PLD) [7]. It substitutes for the selenium compound in various amounts, after samples were ready, they were flattened into  $1 \times 1$  cm discs and placed on a glass substrate that was  $7 \text{ cm} \times 2.5 \text{ cm}$  in size. The system contained a mechanical rotational pump for gas removal as well as a bell constructed of pyrex glass that was 1 mm thick, 320 mm in diameter, and 45 cm high as shown in [8].

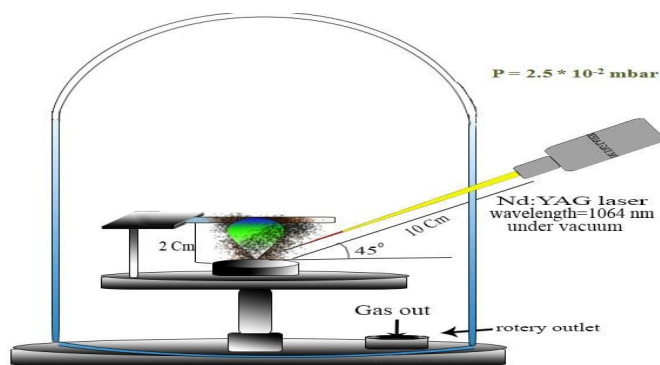


Fig. 1. Illustration of the PLD system used in this work.

The numbers of pulses, as well as, the pulse energy and laser spot size are all configurable. They fluctuate depending on the distance between the laser lens and the target. Use the laser beam to direct the beam at the target at a 45-degree angle. The optical characteristics of the thin films were calculated using 2 g of the target material,  $As_{60}Cu_{40-x}Se_x$  at ( $x = 0, 5, 15$  and  $20$ ) Ultraviolet Visible Spectro- photometer within the wavelength between (300 and 1100 nm).

## 3. Results and discussion

### 3.1. Optical properties

#### 3.1.1. Transmittance spectrum

The results of examining the transmittance and absorption spectrum of  $As_{60}Cu_{40-x}Se_x$  at ( $x = 0, 5, 10, 15$  and  $20$ ) for the thin film at wavelengths between (300 and 1100 nm) revealed that the transmittance increases with increasing wavelength and decreases with increasing distortion, as shown in figure 2. The cause of this is the formation of motional levels inside the energy gap as a result of replaced, which increases the membrane's absorbance and decreases the transmittance of the membrane.[9].

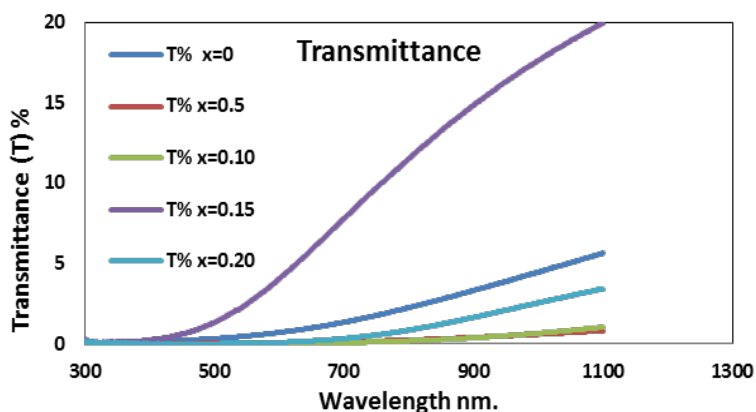


Fig. 2. Transmittance as a function of wavelength  $As_{60}Cu_{40-x}Se_x$  Thin film with  $X = 0.20, 0.15, 0.1$  and  $0.5$

### 3.1.2. Absorbance spectrum

In the case of absorbance, we note that its absorption curves behave exactly the opposite of the transmittance curves, and decrease with increasing wavelength at longitudinal wavelengths (at low energies). At short wavelengths (at higher energies), the absorbance changes with increasing doping, as in Figure 3.

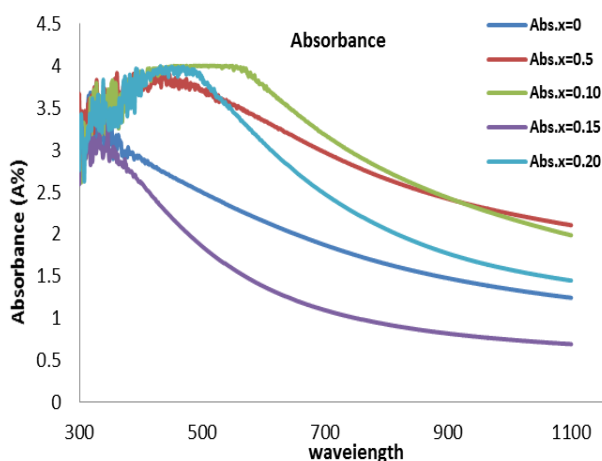


Fig. 3. Absorbance as a function of wavelength ( $As_{60}Cu_{40-x}Se_x$ ) Thin film with different Se concentration.

### 3.1.3. Energy gap

The energy necessary to excite electrons from top of the valence band to bottom of the conduction band is termed as the gap energy (48) and it has been called prohibited or forbidden because the time period during which the electron possesses energy during this region is very short (93) and it is considered the most important optical constant on which semiconductors are relied upon for the manufacture of many electronic devices such as solar cells, detectors, photodiodes and others. The energy gap was calculated by drawing the graphic relationship between  $(\alpha h\nu)^2$  and  $(h\nu)$  as in figure 4 ( $x = 0, 5, 10, 15$  and  $20$ ) and the energy gap is calculated when  $(\alpha h\nu)^2 = 0$  of the intersection of the tangent with  $(h\nu)$ . The point of intersection represents the energy gap and we note that the values of the energy gap decrease with distortion and the schedule 1 represents energy gap computations with increasing concentration [10,11].

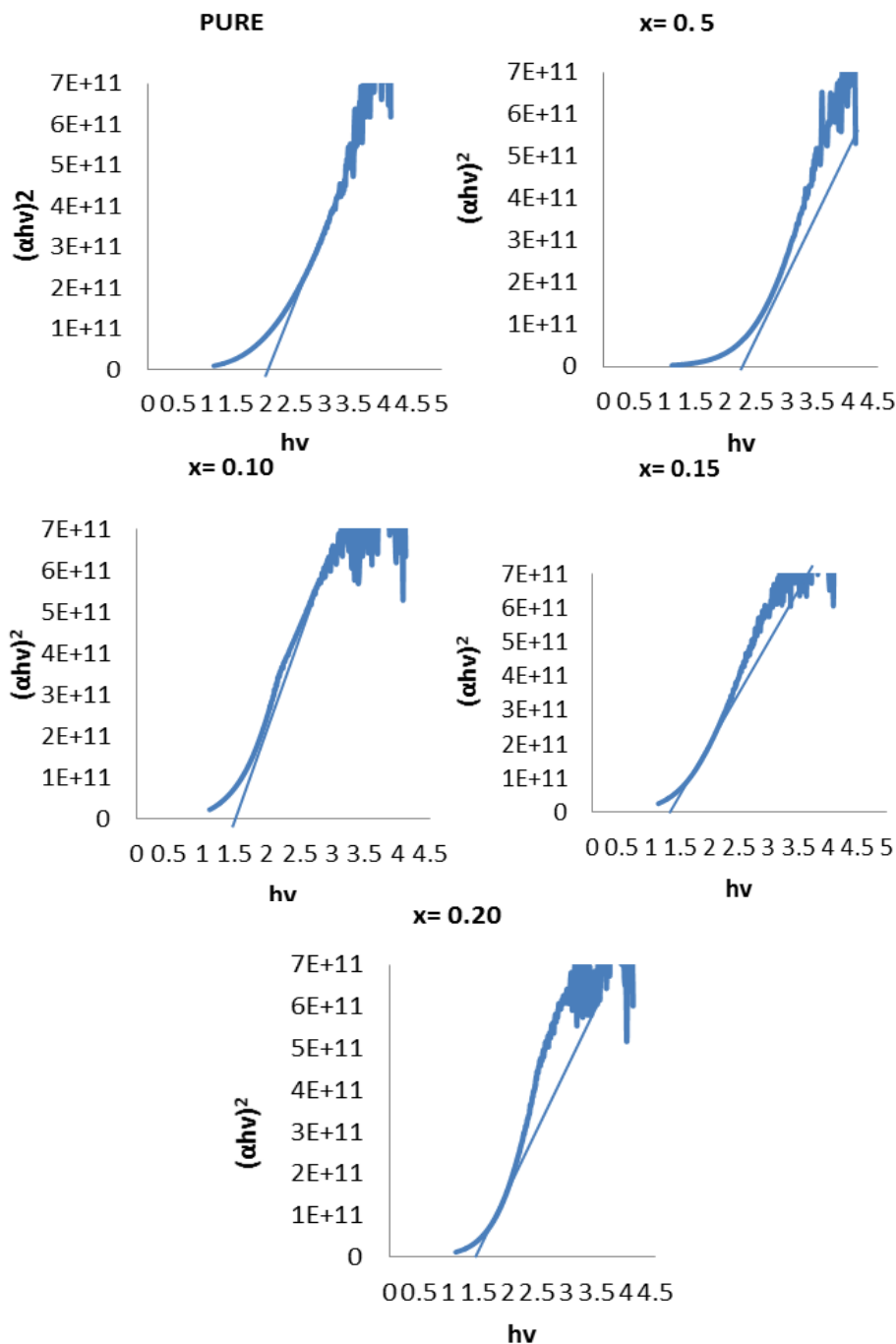


Fig. 4. Energy gap of  $(As_{60}Cu_{40-x}Se_x)$  Thin film  $x=0$  (pure), 0.5, 0.10, 0.15 and 0.20.

Table 1. Represents the values of the energy gap with  $x=0$  (pure), 0.5, 0.10, 0.15 and 0.20.

Se concentration (x)	X=0	X=0.5	X=0.10	X=0.15	X=0.20
energy gap (Eg)	2.5	2.4	1.5	1.4	1.3

### 3.2. Electrical properties

Continuous electrical measurements when temps. are low, medium, and high were examined for the five samples just partially replacement of Se with Cu showing in figure 5. All materials are electrically conductive alloy at various temperatures, thin films were with semiconductor behavior (i.e. all samples increased with electrical conductivity with temperature

increase) . Figure 5 shows the relationship between the logarithm of electrical conductivity and temperature . From this figure , it can be seen that every sample's conductivity depends on the temperature and behavior of the semiconductor as temperature rise , electrical conductivity rise as well as illustrating how each alloy operates as a semiconductor [12] . Additionally , as amount of Se raises the electrical conductivity rises . In order to identify probable the processes in the thin films , informations of the conductivity were analyzed , in particular procedures of the electrically stimulated shown between  $\ln$  versus  $1000/T$  for the  $As_{60}Cu_{40-x}Se_x$  compound . The curves of all the samples under the experiment demonstrate that there are three different ways that electrical stimulation affects conduction . as each curve consists of three different parts for each part has its own activation energy obtained before the exponential factors according to equation 1 which represents the conduction mechanisms for all regions levels [13,14]

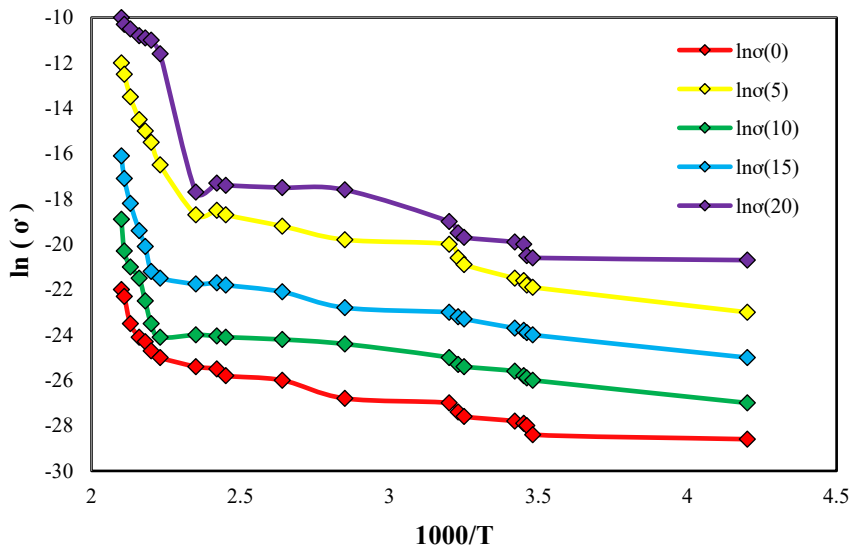


Fig. 5. Representing the relationship between the logarithm of the DC electrical resistance ( $\ln \sigma$ ) and the reciprocal of the absolute temperature ( $1000 / T$ ) for the compound  $As_{60}Cu_{40-x}Se_x$  with  $x= 0, 5, 10, 15$  and  $20$

The activation energies  $\Delta E_3$  ,  $\Delta E_2$  and  $\Delta E_1$  and the pre-exponential factor  $\sigma_{01}$ ,  $\sigma_{02}$  and  $\sigma_{03}$  were calculated for each of these parts , respectively . They are listed in table 1. The interaction of activation energies  $\Delta E_1$  ,  $\Delta E_2$  and  $\Delta E_3$  and Se concentration was drawn in the figure 6. Through this figure, it is noticed that the  $\Delta E_1$  ,  $\Delta E_2$  and  $\Delta E_3$  of These findings concur with those of the researchers in reference , who found that all samples rise with increasing Se content .

Table 2. The composition dependence of activation emerges ( $\Delta E_1, \Delta E_2, \Delta E_3$ ) and pre- exponential factor  $\sigma_{0ext}, \sigma_{0loc}, \sigma_{0loc}$  for three regent states of  $As_{60}Cu_{40-x}Se_x$ .

	High temperature		medium temperature		low temperature	
$X$	$\Delta E_1 (eV)$	$\sigma_{01} \times 10^{-5} (\Omega.cm)^{-1}$	$\Delta E_2 (eV)$	$\sigma_{02} \times 10^{-5} (\Omega.cm)^{-1}$	$\Delta E_3 (eV)$	$\sigma_{03} \times 10^{-5} (\Omega.cm)^{-1}$
0	5.7	27.85	1.2	2.403	0.16	1.935
5	5.9	24,032	1.7	19.35	0.12	1.999
10	6.1	2.696	2.9	2.779	0.125	9.995
15	6.7	2.394	3.7	36.64	0.157	2.593
20	6.9	2.3966	4.7	10.79	1.9	4.999

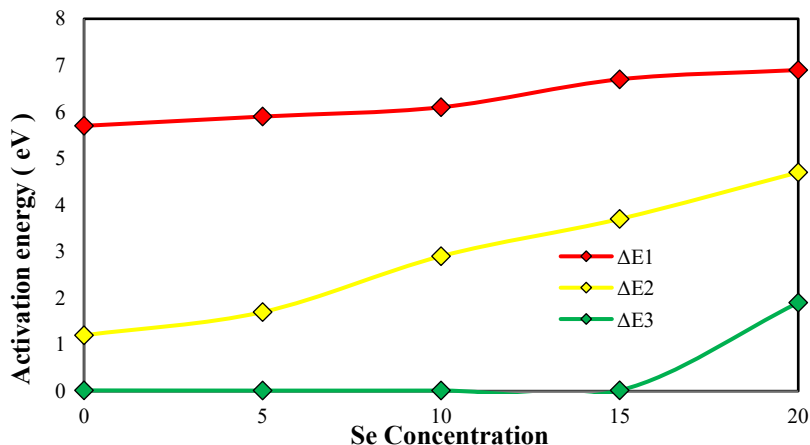


Fig. 6. Shows the Activation Energy as a function of Se concentration for  $As_{60}Cu_{40-x}Se_x$  ( $x = 0, 5, 10, 15$  and  $20$ ).

Figure 7 shows dimension of hopping ( $R$ ), domain of energy tail ( $\Delta E$ ), also distance between atoms ( $a$ ) which are calculated from the theoretical components' equations as a function of Se element concentration, where it is typically seen that both  $R$  and  $E$  decrease with increasing concentration of element Se, this indicates the presence of condensation in the band's energy levels, and thus these variables dropped. Additionally, the decline in local states results in the compound's propensity to crystallize the state, moving away from randomness, as shown in table 2.

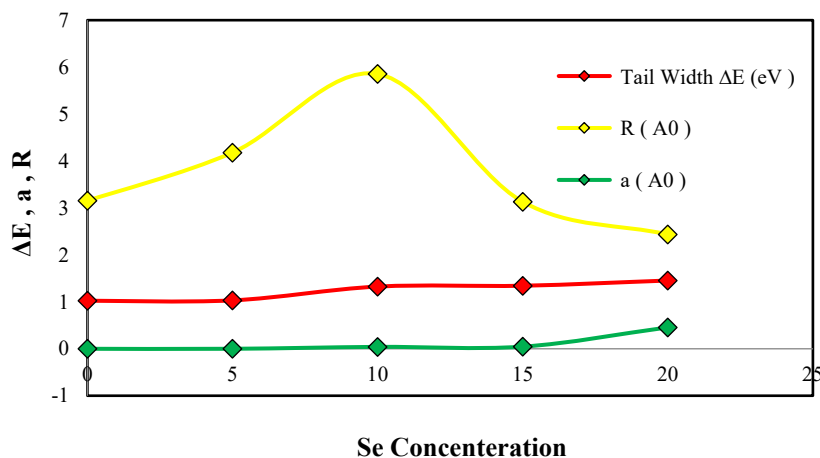


Fig. 7 : Displays dimension of hopping ( $R$ ), domain of energy tail ( $\Delta E$ ) and distance between atoms ( $a$ ) versus of Se concentration for  $As_{60}Cu_{40-x}Se_x$  with  $x = 0, 5, 10, 15$  and  $20$ .

For all samples, it is noted from table 2 that the raise in Se content ( $x = 0, 5, 10, 15$ ) for the samples leads to an increase in energy levels in the extended states  $N$  ( $E_{ext}$ ) and this indicates that the atomic structure of the samples becomes more regular at these concentrations [10], but it decreases at the concentration 20, and this is reflected in the density of cases. The locality at the tails of the bundles ( $E_{loc}$ ) with the raise in Se content as shown in the figure 8, and this shows that the randomness increases with the increase in the concentration of selenium at 20, and at the same time it is noted that there is a slight change in the Fermi level's state density ( $E_f$ ) with a rise in selenium concentration. This indicates that the randomness in the configuration has decreased significantly [13]. They are illustrated in figure 8 and shown in table 3.

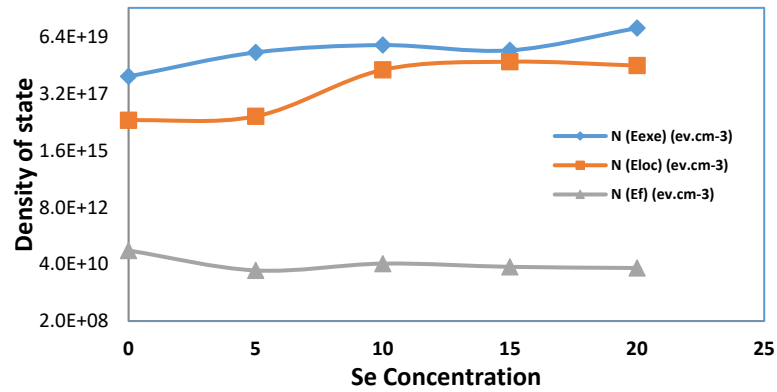


Fig. 8. Represents the densities of energy states with respect to Se concentration for  $As_{60}Cu_{40-x}Se_x$ .

Table 3. Represents to Tail Width  $\Delta E$ ,  $R$  and  $a$ , as well as the density of states for the three reigns.

X	$\Delta E$ (eV)	$R$ ( $\text{\AA}^0$ )	$a$ ( $\text{\AA}^0$ )	$N_{(Eext.)} \times 10^{18}$ ( $1/\text{eV.cm}^3$ )	$N_{(Eloc.)} \times 10^{16}$ ( $1/\text{eV.cm}^3$ )	$N_{(Ef)} \times 10^{10}$ ( $1/\text{eV.cm}^3$ )
0	1.024	3.15466	$3.9178 \times 10^{-3}$	1.654	2.75	14.5
5	1.031	4.17911	$4.540 \times 10^{-3}$	15.566	40	2.26
10	1.325	5.8543	0.04047	30.87	306	4.28
15	1.343	3.1314	0.04557	18.94	656	3.16
20	1.454	2.4358	0.45522	1.51	4.57	2.84

#### 4. Conclusion

This study focused on the effect of partial substitution of copper with selenium on the electrical properties of  $As_{60}Cu_{40-x}Se_x$  ( $x = 0, 5, 10, 15, 20$ ). This study confirmed the existence of three conduction mechanisms: localized state conduction at medium temperatures, extended state (high-temperature conduction temperatures) and localized (variable band jumping near plane of Fermi in the little temperature). The high, middle and little temperature regions of the samples and electrical conductivity measurements were separated for the purpose of determining the conductivity coefficients, the density of the localized and extended states at the beam tails of the medium. has been calculated three conduction processes were identified by electrical measurements: extended-state conduction the temperature is high to localized conduction in the middle temperature and band-variable jumping in the little temperature.

The introduction of selenium had the effect of increasing the activation energy of the expanded status conduction in plane of Fermi and decreasing the activation dose in the localized vacuum states. This effect was measured as a function of concentration. It was found that increasing the concentration of selenium in the samples led to a clear change in all conduction coefficients and in the intensity of the local and extended state and at the Fermi level. As for the optical properties such as absorbance, transmittance and energy gap, the consequences pointed that raising concentration of the selenium guide to a clear change in all optical properties.

## References

- [1] Ashfold, M. N., Claeysens, F., Fuge, G. M., & Henley, S. J. (2004). Pulsed laser ablation and deposition of thin films. *Chemical Society Reviews*, 33(1), 23. <https://doi.org/10.1039/b207644f>
- [2] Heera, P., & Sharma, R. (2014). Effect of Sn on the dielectric properties of te rich se-te glassy alloys. *AIP Conference Proceedings*. <https://doi.org/10.1063/1.4872764>.
- [3] Mott, N. F., & Davis, E. A. (2012). *Electronic processes in non-crystalline materials*. Oxford University Press.
- [4] Abdulateef, A. N., Alsudani, A., Chillab, R. K., Jasim, K. A., & Shaban, A. H. (2020). Calculating the Mechanisms of Electrical Conductivity and Energy Density of States for Se<sub>85</sub>Te<sub>10</sub>Sn<sub>5</sub>-xIn<sub>x</sub> Glasses Materials. *Journal of Green Engineering (JGE)*, 10(9), 5487-5503..
- [5] Ahmed, B. A., Mohammed, J. S., Fadhil, R. N., Jasim, K. A., Shaban, A. H., & Al Dulaimi, A. H. (2022). The dependence of the energy density states on the substitution of chemical elements in the se<sub>6</sub>te<sub>4</sub>-xsbx thin film. *Chalcogenide Letters*, 19(4), 301-308. <https://doi.org/10.15251/cl.2022.194.301>
- [6] Khudhair, N. H., & Jasim, K. A. (2023). A study of the effectiveness of tin on the thermal conductivity coefficient and electrical resistance of se<sub>60</sub>te<sub>40</sub>-xs<sub>n</sub>x Chalcogenide glass. *Ibn AL-Haitham Journal For Pure and Applied Sciences*, 36(1), 149-157. <https://doi.org/10.30526/36.1.2892>
- [7] Omata, T., Nose, K., & Otsuka-Yao-Matsuo, S. (2009). Size dependent optical band gap of ternary I-III-VI<sub>2</sub> semiconductor nanocrystals. *Journal of Applied Physics*, 105(7), 073106. <https://doi.org/10.1063/1.3103768>
- [8] Dwech, M. H., Aadim, K. A., & Mohsen, M. T. (2019, August). The effect of a number of laser pulses on optical properties of CuO thin films deposited by pulsed laser deposited (PLD) technique at 673K. In *AIP Conference Proceedings* (Vol. 2144, No. 1, p. 030024). AIP Publishing LLC.. <https://doi.org/10.1063/1.5123094>
- [9] Chillab, R. K., Jahil, S. S., Wadi, K. M., Jasim, K. A., & Shaban, A. H. (2021). Fabrication of Ge<sub>30</sub>Te<sub>70</sub>-xSbx Glasses alloys and studying the effect of partial substitution on D.C electrical energy parameters. *Key Engineering Materials*, 900, 163-171. <https://doi.org/10.4028/www.scientific.net/kem.900.163>
- [10] Khudhair, N. H., & Jasim, K. A. (2023). Preparation and study the effective of Sb on the energy density of states of Se<sub>60</sub> Te<sub>40</sub>. *TECHNOLOGIES AND MATERIALS FOR RENEWABLE ENERGY, ENVIRONMENT AND SUSTAINABILITY: TMREES22Fr*. <https://doi.org/10.1063/5.0129550>
- [11] Sharma, V., Thakur, A., Goyal, N., Saini, G. S., & Tripathi, S. K. (2004). Effect of in additive on the electrical properties of se-te alloy. *Semiconductor Science and Technology*, 20(1), 103-107. <https://doi.org/10.1088/0268-1242/20/1/017>
- [12] Jassim, G., Obeid, A., & Al Nasheet, H. A. (2018). Knowledge, attitudes, and practices regarding cervical cancer and screening among women visiting primary health care centres in Bahrain. *BMC Public Health*, 18(1). <https://doi.org/10.1186/s12889-018-5023-7>
- [13] Zainab, J., Jasim, K. A., Kadhum, F. J., & Shaban, A. H. (2021). Heat treatment at different temperatures and its effect on the optical properties of pure PMMA and PMMA-coumarin. *Key Engineering Materials*, 900, 42-47. <https://doi.org/10.4028/www.scientific.net/kem.900.42>

- [14] Kadhim, B. B., Risan, R. H., Shaban, A. H., & Jasim, K. A. (2019). Electrical characteristics of nickel/epoxy - Unsaturated polyester blend nanocomposites. AIP Conference Proceedings. <https://doi.org/10.1063/1.5116989>